ADVANCED FUNCTIONAL MATERIALS
www.afm-journal.de

Oriented Assembly of Gold Nanorods on the Single-Particle Level

*Cyrill Kuemin, Lea Nowack, Luisa Bozano, Nicholas D. Spencer, and Heiko Wolf**

Non-spherical colloidal nanoparticles have great potential for applications owing to their enhanced directional properties. However, the lack of methods to precisely assemble them on surfaces has hindered exploitation of their properties for planar devices. Here, the oriented assembly of short gold nanorods with lengths below 100 nm from colloidal suspensions is demonstrated. A locally induced phase transition confines the colloidal nanorods at a receding three-phase contact line that is controllably moved over a nanostructured surface in a capillary assembly process. Dedicated topographical trapping sites allow for aligned assembly of the nanorods on the single-particle level. The feasibility of this method is demonstrated by assembling nanorods into long-range-ordered, non-close packed arrays that could serve as anti-counterfeit labels by virtue of their distinct optical appearance in the far-field. Furthermore, oriented nanorod dimers that are deterministically assembled have the potential to function as nano-plasmonic antenna devices.

1. Introduction

Wet-chemically synthesized nanoparticles play an important role in the advancement of nanotechnology. In particular, shape-anisotropic metal nanoparticles have been investigated most thoroughly owing to their intriguing combinations of tuneable physicochemical properties.[1–9] Colloidal gold nanorods are commonly obtained by seed-mediated synthesis using cetyltrimethylammonium bromide (CTAB) as a growth-directing ligand.[1] The tuneable aspect ratio of the nanorods, intimately linked to their optical properties, and the possibility to spatio-selectively alter the surface properties by ligand substitution,[10,11] have moved gold nanorods into the focus of current research aiming at the bottom-up creation of novel materials and devices by self-assembly. As a consequence of their anisotropy, colloidal nanorods are subject to directional interactions, providing a handle for tuning the nanoscale forces that govern self-assembly processes.[12] Most importantly, the capability of oriented assembly will potentially allow the unique directional properties of gold nanorods to be harnessed, both on the single-particle level and in ordered assemblies.

Many self-assembly processes in solution have recently been developed toward this goal. For example, oligonucleotide-functionalized gold nanorods have been demonstrated to self-assemble into extended crystals upon addition of DNA linkers. The linker length is by far the major factor controlling the lattice parameters.[13] Long-range orientational order has also been obtained by dispersing nanorods in aligned liquid-crystal hosts.[14] Not only the rod-like shape but also the patchiness of the nanorod surface has been used to induce directional interactions.[15,16] Hydrophobic interactions between polystyrene chains tethered to the ends of otherwise hydrophilic nanorods have been shown to trigger self-assembly in selective solvents.[11,17] While these approaches demonstrate oriented assembly in solution, many nanorod-based applications require ordered nanorod assemblies on substrates. Examples include biosensors,[18] metamaterials[19] and optical nano-antennas for white-light generation,[20] photon steering,[21,22] and trapping of nanoparticles[23] or Escherichia coli bacteria.[24] Strikingly, devices that require long-range ordered, oriented arrangements of nanorods have so far been fabricated by top-down approaches, because self-assembly methods including directed self-assembly approaches that use static or dynamic electric fields,[25,26] molecular scaffolds,[27] interfacial[28] or other types of templates, have not yet advanced to the required level of placement and alignment precision. However, top-down fabricated devices suffer from limited resolution, little control over the surface chemistries, as well as structural imperfections (polycrystallinity, roughness) that directly corrupt the device performance.[29,30] To overcome these limitations, a patterning process is proposed, which employs top-down-fabricated nanostructured templates for the oriented assembly of bottom-up synthesized, colloidal gold nanorods.

C. Kuemin, L. Nowack, Dr. H. Wolf
IBM Research–Zurich
Säumerstrasse 4, CH-8803 Rüschlikon, Switzerland
E-mail: hwo@zurich.ibm.com
C. Kuemin, L. Nowack, Prof. N. D. Spencer
Laboratory for Surface Science and Technology
Department of Materials
ETH Zurich, Wolfgang-Pauli-Strasse 10, CH-8093 Zürich, Switzerland
Dr. L. Bozano
IBM Research–Almaden
650 Harry Road, San Jose, CA 95120-6099, USA

DOI: 10.1002/adfm.201101760

© 2012 WILEY-VCH Verlag GmbH & Co. KGaA, Weinheim

2. Results and Discussion

2.1. Phase-Transition-Mediated Confinement of Nanorods

The proposed patterning method relies on the strong spatial confinement of the nanorods at the three-phase contact line of a colloid drop that is placed and slowly moved (velocity $v = 0.5–1\ \mu ms^{-1}$) over a nanostructured template surface in a capillary-assembly process (see Experimental Section for details).[31–35] Colloidal suspensions of cetyltrimethylammonium bromide (CTAB)-stabilized gold nanorods with approximate dimensions of 25 nm × 80 nm are considered. The concentration of CTAB, which also serves as cationic surfactant, is adjusted to c_{CTAB} = 0.9 mM, resulting in a meniscus profile as schematically depicted in **Figure 1**a and an initial contact angle of 50 ± 3° when hydrophobic poly(dimethylsiloxane) (PDMS) templates are used. CTAB is also adsorbed on the nanorod surface as a self-assembled bilayer that exposes positively charged ammonium ions to the liquid phase.[36] In this way, CTAB induces electrical-double-layer forces that provide colloidal stability.

Initially, the nanorods undergo rapid rotational and translational diffusion in the bulk as well as near the receding three-phase contact line, where the latter is evidenced by microscopic examination. To suppress the randomizing effect of Brownian motion—a requirement for high-yield assembly[34]—the nanorods are subject to a two-step confining procedure as the colloid drop moves over the template surface. In the first step, where the temperature of the colloidal suspension is maintained at 30–35 °C, a convective flux of liquid toward the three-phase contact line is established by controlled evaporation of water from the meniscus. The nanorods are sufficiently large to experience the long-range hydrodynamic force-field superimposed on the stochastic Brownian forces. In effect, nanorods accumulate near the three-phase contact line (Figure 1a, left). The formation of a high-concentration zone, which we termed the accumulation zone, can be observed microscopically by an increase in the intensity of red light resonantly scattered from the nanorods under dark-field illumination. The fluctuating scattered intensity (see Supporting Information Movie)—and the fact that the accumulation zone appeared identical when viewed through a polarizer at different orientations—suggest that the nanorods are in an isotropic phase at this stage. Figure 1b (left) shows a dark-field optical microscopy image of the meniscus area with an isotropic accumulation zone.

In the second step of the confining procedure, the accumulated nanorods in the isotropic state are subject to a phase transition, effected by increasing the colloid temperature to 50–55 °C (Figure 1a, right). As the colloid temperature and the liquid flux are connected by a power law, the nanorod volume fraction at the contact line rapidly increases.[34] Eventually, a second phase nucleates at the contact line and grows into ordered domains separated by a distinct phase boundary from the isotropic phase toward the bulk. The dark-field images in Figure 1b (right) show these domains. Thermal cycling nucleates and dissolves the domains, which indicates the presence of equilibrium phases. Furthermore, the domains exhibit striking optical anisotropy, changing their color from orange-red to green when viewed through a polarizer at 0° to 90° orientation with respect to the contact line, indicating orientationally ordered nanorods.

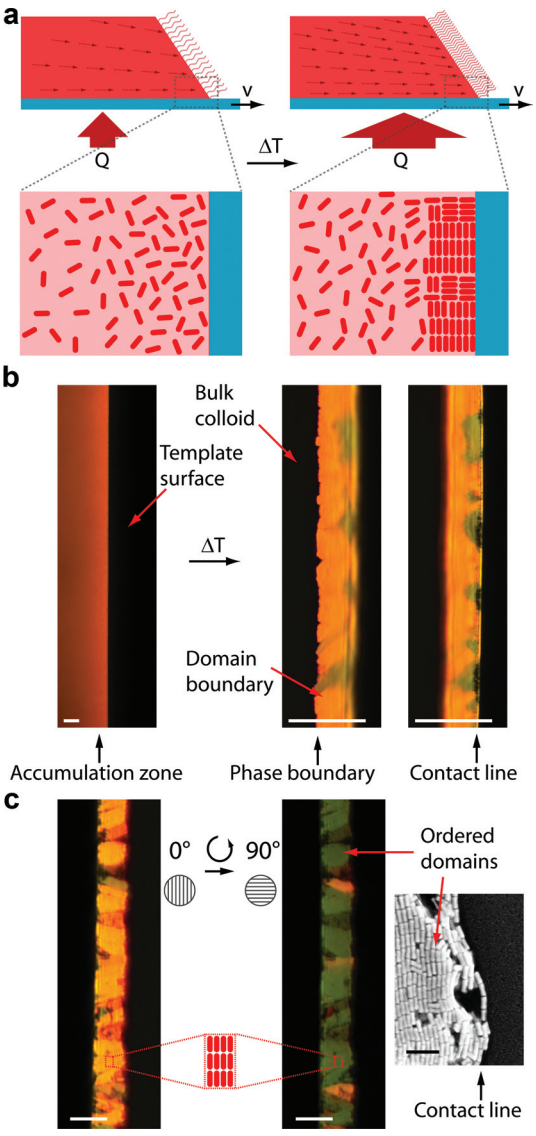

Figure 1. Phase transition-mediated confinement of nanorods. a) A colloid drop (red) is moved over the template (blue) at a velocity v. Water evaporates from the meniscus as a result of the heat Q supplied to the colloid. Convection causes transport of the dispersed nanorods to the three-phase contact line, where an accumulation zone is formed. Raising the colloid temperature by ΔT increases the nanorod concentration, and leads to a phase transition near the contact line and confines the nanorods. b) Dark-field optical microscopy images of the accumulation zone in the isotropic phase *I* (left) and the solid phase *S* (right). The solid domains extend from the contact line to the phase boundary; both are set in focus in the two images. c) The domains appear orange-red or green when viewed through a polarizer depending on the relative orientation of the transmission direction to the orientationally ordered nanorods that comprise the domains. The scale bars are 25 µm. The electron microscopy image shows the ordering of the nanorods in the dry state (scale bar: 200 nm).

Colloidal suspensions of rod-like particles have indeed been observed and predicted to exhibit rich phase behaviour owing to excluded-volume effects that are a direct consequence of the

© 2012 WILEY-VCH Verlag GmbH & Co. KGaA, Weinheim

particle anisotropy.[37] Computer simulations of hard spherocylinders as model particles (l: length of the cylinder, D: diameter of the cylinder) predict a coexistence region of an isotropic with an orientationally ordered, crystalline solid phase at shape anisotropies $\frac{l}{D} < 3.1$.[38] To account for the presence of charges on the particle surface, effective dimensions have recently been computed for charged spherocylinders.[39] The corresponding phase diagram has been assumed to follow from hard spherocylinders with effective dimensions. Essentially, charged spherocylinders behave less anisotropically than their hard counterparts. The CTAB-stabilized gold nanorods considered in this work have a shape anisotropy $\frac{l}{D} = 2.2$ and the screening length of the aqueous dispersant during the observed phase transition is estimated to be $\kappa^{-1} = 6.5$ nm (see Supporting Information). The electrical double layer is thus strongly compressed, the effective shape anisotropy of the charged nanorods differs little from the hard-core value and the corresponding phase diagram predicts a phase transition from the isotropic phase I to an orientationally ordered solid phase S. The prediction of an orientationally ordered phase is in accordance with the observed optical anisotropy of the domains. Based on this observation, the plastic solid phase, which exhibits positional but no orientational order, has been precluded. Liquid-crystalline phases, which also exhibit optical anisotropy, are expected only in suspensions of rods with higher shape anisotropy. Within the domains, the nanorods are aligned along a common director. Moreover, the color of the domains, when viewed through a polarizer, reveals the orientation of the director, because the light scattered from the gold nanorods is perpendicularly polarized with a transversal (green) and a longitudinal component (red). Thus, the domains shown in Figure 1c are predominantly aligned parallel to the contact line, whereas the green domains in the dark-field images of Figure 1b taken without the polarizer indicate upright-oriented nanorods. Upon complete drying of the dispersant, the nanorods have, at least partially, retained the ordered state as evidenced by SEM imaging (see Supporting Information Figure 2) and previously reported in drying-mediated self-assembly processes.[28]

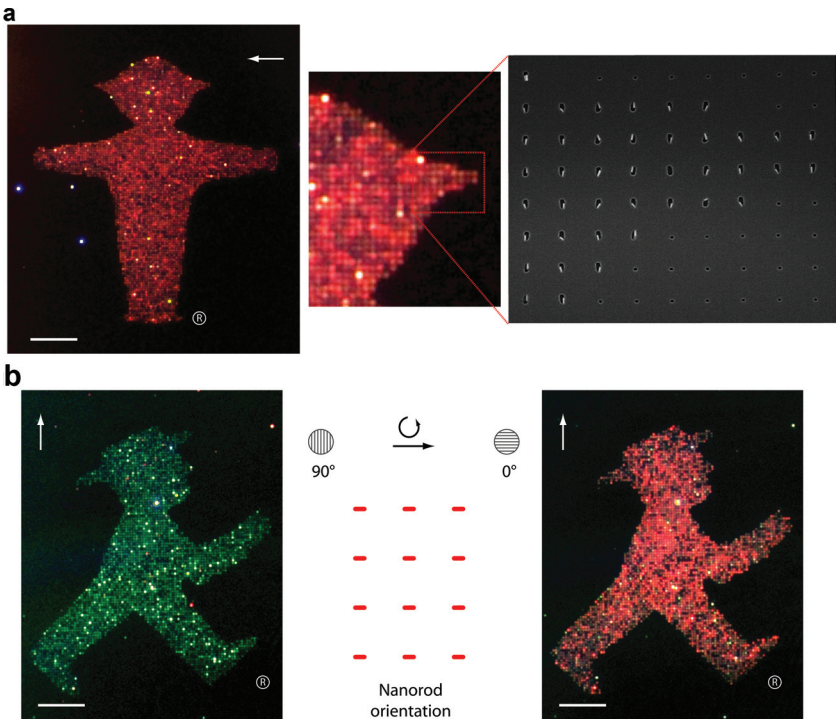

Figure 2. Aligned nanorods in recessed linelets in PDMS templates. a) Gold nanorods are arranged to display the STOP Ampelmann, which is 50 µm × 60 µm in size. The arrows indicate the traveling direction of the meniscus in the assembly process. The nanorods, which constitute the individual pixels of the image, are placed with single-particle resolution in linelets measuring 50 nm × 140 nm in size. The assembly yield is larger than 95%. The pixels are separated by 500 nm. The round holes placed next to the linelet array serve as pinning features. b) Dark-field optical microscopy images of the WALK Ampelmann were recorded through a polarizer. The pixels change their color from green to red as the polarizer is rotated by 90°. The scale bars are 10 µm. (The AMPELMANN is a registered trademark of the AMPELMANN GmbH.)

2.2. High-Yield Oriented Assembly

The liquid-air boundary associated with capillary forces and the mutual confinement within the three-dimensionally ordered domains strongly reduce the mobility of the nanorods at the three-phase contact line, providing favorable conditions for high-yield capillary assembly. Oriented assembly of gold nanorods is achieved by moving the solid domains, shown in Figure 1b and c, over nanostructured templates that have arrays of 37 ± 2 nm deep, topographical capturing features, denoted as linelets in the following, on their surface (see Experimental and Supporting Information for details on design and fabrication). To this end, the forced phase transition is synchronized with the moving contact line approaching an array of linelets. Importantly, the capillary forces at the receding liquid-air interface have to be sufficiently strong to maintain the domains in the wet state and to avoid non-specific deposition of nanorods. This condition is met on hydrophobic PDMS with its low surface energy $\gamma \approx 22$ mJ m^{-2}.[40] We measured receding wetting angles of 35 ± 3°, which indicates that dragging the domains across the surface is subject to significant frictional forces.

Under these process conditions, the confined nanorods assemble inside recessed linelets having lateral dimensions of 52 ± 3 nm × 138 ± 3 nm (designed dimensions: 50 nm × 140 nm) and a depth of 37 ± 2 nm. **Figure 2** shows long-range ordered arrays of aligned nanorods, arranged to display the Berlin STOP and WALK Ampelmann. These two traffic light figures were assembled by moving the contact line along the direction indicated by the white arrows. Figure 2a shows a dark-field optical microscopy image of the STOP Ampelmann and a detail of its head. Individual gold nanorods, which strongly scatter red light, constitute the discernible pixels. The assembly yield, as determined on the part of the array that defines the head, is greater than 95%. The bright white spots indicate nanorod dimers. The electron microscopy image demonstrates that the nanorods were

© 2012 WILEY-VCH Verlag GmbH & Co. KGaA, Weinheim

placed in an oriented fashion with single-particle resolution. Figure 2b displays the WALK Ampelmann, imaged through a polarizer at different orientations (90° and 0°) relative to the long axis of the linelets. On the left, the polarizer is oriented parallel to the short axis of the assembled nanorods. Thus, green light that couples to the transversal plasmon resonance is transmitted through the polarizer and vice versa for the "red" WALK Ampelmann. The weak green background is a result of the long exposure time (~800 ms) needed to record the image. The narrow distribution of the orientation of the assembled nanorods is manifested in the predominance of either the green or red color. Only a few pixels have the "wrong" color due to their misorientation.

Initially, we hypothesized that high yields can only be obtained when the long axis of the linelets is oriented parallel to the moving contact line, because the first rows of nanorods at the meniscus are always found being aligned parallel to the contact line (see Supporting Information Figure 2). However, we observed that the nanorods assemble in both the parallel and perpendicular linelets with similar yields. During capillary breakup, when the contact line is being ripped away from the linelet, the assembling nanorod must experience an angular constraint which aligns it into the corresponding linelet. Hence, the pre-alignment of the nanorods in the solid domains is not a prerequisite for successful assembly whereas the dense packing is essential. Virtually no nanorods assembled from an isotropic accumulation zone. **Figure 3**a shows electron microscopy images of nanorods, which were co-assembled in 0°- and 90°-linelets. In terms of the resulting assembly yield, it is critical to have sufficiently large linelets in order to induce contact line pinning. (50 nm × 140 nm)-linelets provide high assembly yields whereas low yields result when the meniscus is moved over an array of (40 nm × 100 nm)-linelets.

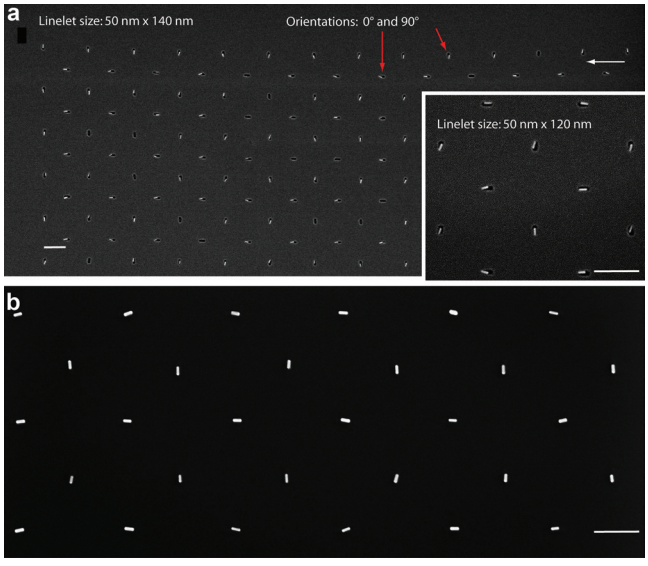

Figure 3. Co-assembled gold nanorods with two orientations. a) Electron microscopy images of gold nanorods aligned in linelets, which are oriented parallel or perpendicular to the receding contact line during assembly. The white arrow indicates the traveling direction of the contact line. b) Gold nanorods printed from (50 nm × 140 nm)-linelets in PDMS onto PMMA-coated silicon substrates. The nanorods retain their relative position and alignment upon printing. The scale bars are 500 nm.

To quantify the accuracy of alignment, we analyzed the orientational distribution of nanorods assembled in the two populations (0°- and 90°-orientation). For this purpose, the assembled nanorods were transferred to PMMA-coated silicon substrates by microcontact printing.[34] The presence of a stiff, conducting substrate was necessary to enable high-resolution electron microscopy imaging of the nanorods. Figure 3b shows an array of printed gold nanorods. Using electron microscopy and image-analysis software, the alignment angle α of the assembled nanorods can be determined (see Supporting Information). The histograms in **Figure 4** show the orientational distribution of the assembled nanorods. The number of nanorods (occurrence) at varying alignment angles α is plotted. The histograms

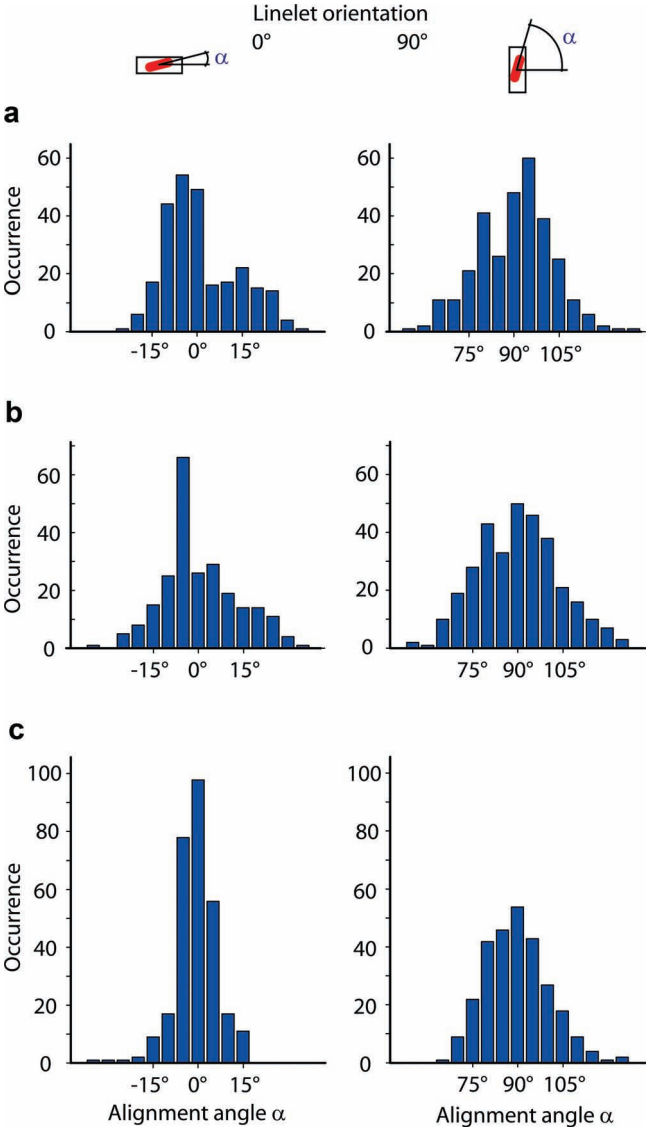

Figure 4. Orientational distributions of aligned nanorods. The distributions of the alignment angle α of nanorods assembled in a) (50 nm × 140 nm)-, b) (50 nm × 120 nm)-, c) and (50 nm × 100 nm)-linelets. The histograms on the left/right include the nanorods in the 0°/90° linelets, respectively. The width of the histogram bars is 5°.

© 2012 WILEY-VCH Verlag GmbH & Co. KGaA, Weinheim

are centred near the target orientations 0° (left histograms) or 90° (right histograms) and decay quickly for alignment angles α larger than 15°. There is no clear trend toward a more narrow distribution for either of the two target orientations for any linelet size. However, shorter linelets provide a stronger angular constraint on the assembling nanorods as indicated by the narrower distribution of the histograms in Figure 4c. As derived from the data in the histogram at the bottom left, 80% of the nanorods in the (50 nm × 100 nm)-linelets at 0° orientation, assembled with an alignment angle between –7° and 7°.

2.3. Deterministic Assembly of Nanorod Dimers

Besides sparse arrays, the presented method also allows the assembly of complex multi-particle structures, for example arrays of oriented nanorod dimers in a co-aligned configuration. Deliberately assembled dimers are obtained with linelets that measure approximately 50 nm × 200 nm in size. Upon drying, capillary immersion forces push apart the two assembling nanorods.[41] Gaps result, whose width depend on the actual length of the nanorods and the linelet. **Figure 5**a shows assembled dimers, which can also be printed on silicon with a 30-nm PMMA adhesion layer (Figure 5b). In the inset, a dark-field optical microscopy image of the same dimers is shown. The variations in the aspect ratio of the nanorods, the gap width, as well as the relative orientation, affect the hybridization of the localized surface plasmons and thus their scattering properties.[42] The field enhancement in the gap of spaced nanorods makes dimers interesting for applications in plasmonics, spectroscopy and nanoelectronics.[20,23,24,43,44] Larger rods (30 nm × 85 nm) often assemble into close-packed dimers in an end-to-end configuration, where the gap width is defined by the thickness of the CTAB shell. Capillary forces do not separate the rods, but rather push them together in this case. Figure 5c shows a selection of such nanorod dimers, printed from 50 nm × 200 nm-linelets in PDMS onto PMMA-coated silicon. Frequently, misaligned nanorods were found. By virtue of the narrow gap width, applications in molecular electronics can be envisioned.[45,46]

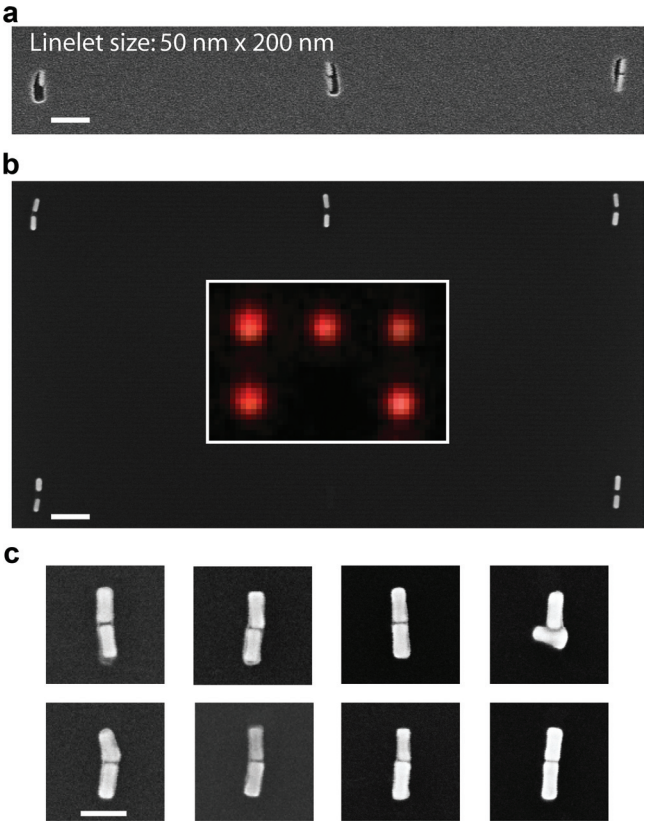

Figure 5. Assembled and printed nanorod dimers. a) A single nanorod (25 nm × 80 nm) and two nanorod dimers assembled in an oriented fashion. The scale bar is 200 nm. b) Arrays of self-assembled nanorod dimers integrated onto silicon substrates by microcontact printing. The inset shows a dark-field optical microscopy image of the same dimers. The scale bar is 200 nm. c) A selection of close-packed 30 nm × 85 nm-nanorod dimers in an end-to-end configuration with narrow gaps. The scale bar is 100 nm.

3. Conclusions and Outlook

The oriented assembly of shape-anisotropic nano-objects has been a heavily studied topic in nanotechnology research. Meanwhile, the development of methods to align carbon nanotubes or silicon nanowires has marked milestones in the field.[47,48] In this paper, we have shown that significantly shorter, shape-anisotropic gold nanorods can be assembled in an oriented fashion, too, by combining top-down surface patterning with a directed self-assembly process. A thorough understanding of the involved phases during assembly has been critical to bias the process toward high assembly yields, while carefully designed assembly templates have afforded oriented assembly and single-particle resolution. By virtue of the placement and alignment capabilities, nanorod arrays have been fabricated with an unprecedented freedom of design, where the directional optical properties of the gold nanorods can be harnessed. The possibility to transfer the assembled arrays by a printing technique makes the process very versatile with respect to the integration of the nanorods into a device. Furthermore, it should be feasible to apply this assembly method to other shape-anisotropic particles, for example to silver or semiconductor nanorods, as capillary forces are not selective for gold nanoparticles. Combining different particle materials and surface chemistries with the alignment capabilities should enable interesting follow-up studies at the forefront of exploratory research in nanotechnology.

4. Experimental Section

Template Fabrication: Nanostructured templates for the oriented assembly of nanorods were fabricated by molding liquid poly(dimethylsiloxane) (PDMS) against a patterned silicon master, fabricated by electron-beam lithography (x'lith GmbH, Ulm, Germany; see Supporting Information for details on pattern design and fabrication). The composition of the PDMS and the replica-molding process have been published previously.[49] Briefly, liquid pre-polymer was sandwiched between the patterned master and a display glass backplane. After curing (48 h, 60 °C), the glass-supported template was manually peeled off from the master. Glass-supported templates were then placed in ethanol for 5 minutes in an ultrasound bath to release

© 2012 WILEY-VCH Verlag GmbH & Co. KGaA, Weinheim

the PDMS template, which was subsequently placed on a silicon carrier and dried for 30 min at 25 mbar. The presence of a silicon surface underneath the transparent PDMS template enhanced the visibility of the patterned area and the nanorods at the meniscus area under dark-field illumination during assembly.

Preparation of Colloidal Suspensions: Colloidal suspensions of gold nanorods were purchased from Nanopartz Inc. (Loveland, CO, USA). The colloidal suspensions contain an unknown amount of cetyltrimethylammonium bromide (CTAB). Therefore, the suspensions were centrifuged (5000 rpm, 10 min) and the supernatant replaced by a CTAB solution of known concentration (c_{CTAB} = 0.9 mM). Colloidal suspensions of gold nanorods in 0.9 mM CTAB solutions were filtered using Millex-LG, 0.2-µm, hydrophilic PTFE pore filters (Millipore, Zug, Switzerland). The filtrate was then centrifuged and the appropriate volume of supernatant removed, to adjust the concentration of the nanorods to $c_{NR} = 10^{12}$ mL^{-1}. The Supporting Information Figure 3 gives the optical extinction spectrum of the colloidal nanorod suspensions.

Two-step Confinement and Capillary Assembly of Nanorods: Capillary assembly of nanorods was performed with a home-built tool, in which the temperature of the colloidal suspension and the velocity v at which the meniscus moves over the template surface can be controlled. The assembly templates were fixed onto a Peltier element, which itself was mounted on a linear translational stage. To carry out an assembly run, 150 µL of colloidal suspension were injected between the template and a stationary silicon slide, which was mounted approximately 1.2 mm above the template. The silicon slides were hydrophobized with dodecyltrichlorosilane (97%, ABCR, Karlsruhe, Germany), adsorbed from the gas phase (10 min, 200 mbar). To ensure completion of the monolayer formation, samples were placed in an oven (1 h, 40 mbar, 80 °C). The silicon slide held the dispensed drop of colloidal suspensions as the assembly templates were moved underneath the colloid drop. To account for changes in the relative humidity in the ambient air, the temperature of the colloidal suspension during the two-step confining procedure was adjusted relative to the dew-point temperature T_{dew}. The experimental setup, mounted on the table of an optical microscope, allowed for visual inspection of the meniscus area from above. Wetting angles were determined on images of the meniscus profile, recorded with a digital camera attached at the side of the setup. The standard deviation of the measured wetting angles was ±3°.

Nanorod Transfer: Nanorods were transferred onto silicon substrates by microcontact printing, carried out using a home-built tool. First, a 30-nm poly(methylmethacrylate) layer (molecular weight 950 kDa, microresist technology GmbH, Berlin, Germany) was spin-coated on the silicon substrate. The PMMA coating served as an adhesion layer. In order to print the nanorods, the PDMS template was brought into contact with the substrate. The temperature was raised to 130 °C and a pressure of approximately 1 bar was applied. After cooling to 40 °C, during which contact was maintained, the PDMS template was removed by lifting off.

Supporting Information

Supporting Information is available from the Wiley Online Library or from the author.

Acknowledgements

Partial financial support from the Swiss National Science Foundation (National Research Program 47 "Supramolecular Functional Materials") is gratefully acknowledged. The authors thank Cathrein Huckstadt and Richard Stutz for technical support, Armin Knoll, Urs Duerig, Felix Holzner, Emmanuel Delamarche and Robert Lovchik for discussions, Michel Despont and Walter Riess for their continuous support, and the AMPELMANN GmbH for providing their designs.

Received: July 29, 2011
Published online: December 6, 2011

[1] N. R. Jana, L. Gearheart, C. J. Murphy, *J. Phys. Chem. B* **2001**, *105*, 4065–4067.
[2] N. Malikova, I. Pastoriza-Santos, M. Schierhorn, N. A. Kotov, L. M. Liz-Marzan, *Langmuir* **2002**, *18*, 3694–3697.
[3] Y. Sun, Y. Xia, *Science* **2002**, *298*, 2176–2179.
[4] C. J. Murphy, T. K. Sau, A. M. Gole, C. J. Orendorff, J. Gao, L. Gou, S. E. Hunyadi, T. Li, *J. Phys. Chem. B* **2005**, *109*, 13857–13870.
[5] A. Tao, P. Sinsermsuksakul, P. Yang, *Angew. Chem. Int. Ed.* **2006**, *45*, 4597–4601.
[6] F. Hao, C. L. Nehl, J. H. Hafner, P. Nordlander, *Nano Lett.* **2007**, *7*, 729–732.
[7] J. Henzie, E. Kwak, T. W. Odom, *Nano Lett.* **2005**, *5*, 1199–1202.
[8] T. K. Sau, A. L. Rogach, F. Jäckel, T. A. Klar, J. Feldmann, *Adv. Mater.* **2010**, *22*, 1805–1825.
[9] T. K. Sau, A. L. Rogach, *Adv. Mater.* **2010**, *22*, 1781–1804.
[10] C. J. Murphy, L. B. Thompson, A. M. Alkilany, P. N. Sisco, S. P. Boulos, S. T. Sivapalan, J. A. Yang, D. J. Chernak, J. Huang, *J. Phys. Chem. Lett.* **2010**, *1*, 2867–2875.
[11] Z. Nie, D. Fava, E. Kumacheva, S. Zou, G. C. Walker, M. Rubinstein, *Nat. Mater.* **2007**, *6*, 609–614.
[12] K. J. M. Bishop, C. E. Wilmer, S. Soh, B. A. Grzybowski, *Small* **2009**, *5*, 1600–1630.
[13] M. R. Jones, R. J. MacFarlane, B. Lee, J. Zhang, K. L. Young, A. J. Senesi, C. A. Mirkin, *Nat. Mater.* **2010**, *9*, 913–917.
[14] Q. Liu, Y. Cui, D. Gardner, X. Li, S. He, I. I. Smalyukh, *Nano Lett.* **2010**, *10*, 1347–1353.
[15] K. K. Caswell, J. N. Wilson, U. H. F. Bunz, C. J. Murphy, *J. Am. Chem. Soc.* **2003**, *125*, 13914–13915.
[16] G. A. DeVries, M. Brunnbauer, Y. Hu, A. M. Jackson, B. Long, B. T. Neltner, O. Uzun, B. H. Wunsch, F. Stellacci, *Science* **2007**, *315*, 358–361.
[17] K. Liu, Z. Nie, N. Zhao, W. Li, M. Rubinstein, E. Kumacheva, *Science* **2010**, *329*, 197–200.
[18] G. J. Nusz, S. M. Marinakos, A. C. Curry, A. Dahlin, F. Höök, A. Wax, A. Chilkoti, *Anal. Chem.* **2008**, *80*, 984–989.
[19] V. M. Shalaev, W. Cai, U. K. Chettiar, H. K. Yuan, A. K. Sarychev, V. P. Drachev, A. V. Kildishev, *Opt. Lett.* **2005**, *30*, 3356–3358.
[20] P. Muhlschlegel, H. Eisler, O. J. F. Martin, B. Hecht, D. W. Pohl, *Science* **2005**, *308*, 1607–1609.
[21] T. Kosako, Y. Kadoya, H. F. Hofmann, *Nat. Photonics* **2010**, *4*, 312–315.
[22] A. G. Curto, G. Volpe, T. H. Taminiau, M. P. Kreuzer, R. Quidant, N. F. van Hulst, *Science* **2010**, *329*, 930–933.
[23] W. Zhang, L. Huang, C. Santschi, O. J. F. Martin, *Nano Lett.* **2010**, *10*, 1006–1011.
[24] M. Righini, P. Ghenuche, S. Cherukulappurath, V. Myroshnychenko, F. J. Garcia de Abajo, R. Quidant, *Nano Lett.* **2009**, *9*, 3387–3391.
[25] B. M. I. van der Zande, G. J. M. Koper, H. N. W. Lekkerkerker, *J. Phys. Chem. B* **1999**, *103*, 5754–5760.
[26] W. Ahmed, E. S. Kooij, A. van Silfhout, B. Poelsema, *Nano Lett.* **2009**, *9*, 3786–3794.
[27] M. A. Correa-Duarte, J. Perez-Juste, A. Sanchez-Iglesias, M. Giersig, L. M. Liz-Marzan, *Angew. Chem. Int. Ed.* **2005**, *44*, 4375–4378.
[28] T. Ming, X. Kou, H. Chen, T. Wang, H. L. Tam, K. W. Cheah, J. Y. Chen, J. Wang, *Angew. Chem. Int. Ed.* **2008**, *120*, 9831–9836.
[29] K. Chen, V. P. Drachev, J. D. Borneman, A. V. Kildishev, V. M. Shalaev, *Nano Lett.* **2010**, *10*, 916–922.
[30] J. Huang, J. S. Huang, V. Callegari, P. Geisler, C. Brüning, J. Kern, J. C. Prangsma, X. Wu, T. Feichtner, J. Ziegler, P. Weinmann, M. Kamp, A. Forchel, P. Biagioni, U. Sennhauser, B. Hecht, *Nat. Commun.* **2010**, *1*, 150.
[31] Y. Yin, Y. Lu, B. Gates, Y. Xia, *J. Am. Chem. Soc.* **2001**, *123*, 8718–8729.

© 2012 WILEY-VCH Verlag GmbH & Co. KGaA, Weinheim

[32] Y. Cui, M. T. Bjork, J. A. Liddle, C. Sönnichsen, B. Boussert, A. P. Alivisatos, *Nano Lett.* **2004**, *4*, 1093–1098.
[33] L. Malaquin, T. Kraus, H. Schmid, E. Delamarche, H. Wolf, *Langmuir* **2007**, *23*, 11513–11521.
[34] T. Kraus, L. Malaquin, H. Schmid, W. Riess, N. D. Spencer, H. Wolf, *Nat. Nanotechnol.* **2007**, *2*, 570–576.
[35] C. Kuemin, R. Stutz, N. D. Spencer, H. Wolf, *Langmuir* **2011**, *27*, 6305–6310.
[36] B. Nikoobakht, M. A. El-Sayed, *Langmuir* **2001**, *17*, 6368–6374.
[37] M. Baus, L. F. Rull, J. Ryckaert, *Observation, prediction and simulation of phase transitions in complex fluids*, Kluwer Academic Publishers, Dordrecht, The Netherlands **1995**.
[38] P. Bolhuis, D. Frenkel, *J. Chem. Phys.* **1997**, *106*, 666–687.
[39] E. Eggen, M. Dijkstra, R. van Roij, *Phys. Rev. E* **2009**, *79*, 041401.
[40] C. J. Drummond, D. Y. C. Chan, *Langmuir* **1997**, *13*, 3890–3895.
[41] M. J. Gordon, D. Peyrade, *Appl. Phys. Lett.* **2006**, *89*, 053112.
[42] L. S. Slaughter, Y. Wu, B. A. Willingham, P. Nordlander, S. Link, *ACS Nano* **2010**, *4*, 4657–4666.
[43] M. L. Pedano, S. Li, G. C. Schatz, C. A. Mirkin, *Angew. Chem. Int. Ed.* **2010**, *49*, 78–82.
[44] Y. Weizmann, J. Lim, D. M. Chenoweth, T. M. Swager, *Nano Lett.* **2010**, *10*, 2466–2469.
[45] J. Liao, L. Bernard, M. Langer, C. Schoenenberger, M. Calame, *Adv. Mater.* **2006**, *18*, 2444–2447.
[46] T. Jain, F. Westerlund, E. Johnson, K. Moth-Poulsen, T. Bjornholm, *ACS Nano* **2009**, *3*, 828–834.
[47] Y. Huang, X. Duan, Q. Wei, C. M. Lieber, *Science* **2001**, *291*, 630–633.
[48] M. Li, R. B. Bhiladvala, T. J. Morrow, J. A. Sioss, K.-K. Lew, J. M. Redwing, C. D. Keating, T. S. Mayer, *Nat. Nanotechnol.* **2008**, *3*, 88–92.
[49] M. Geissler, H. Wolf, R. Stutz, E. Delamarche, U.-W. Grummt, B. Michel, A. Bietsch, *Langmuir* **2003**, *19*, 6301–6311.

© 2012 WILEY-VCH Verlag GmbH & Co. KGaA, Weinheim